Cell

# Structure of DDB1 in Complex with a Paramyxovirus V Protein: Viral Hijack of a Propeller Cluster in Ubiquitin Ligase

Ti Li,[1] Xiujuan Chen,[2] Kenneth C. Garbutt,[1] Pengbo Zhou,[2] and Ning Zheng[1,*]
[1] Department of Pharmacology, Box 357280, University of Washington, Seattle, WA 98195, USA
[2] Department of Pathology and Laboratory Medicine, Weill Medical College of Cornell University, 1300 York Avenue, New York, NY 10021, USA
*Contact: nzheng@u.washington.edu
DOI 10.1016/j.cell.2005.10.033

## SUMMARY

**The DDB1-Cul4A ubiquitin ligase complex promotes protein ubiquitination in diverse cellular functions and is reprogrammed by the V proteins of paramyxoviruses to degrade STATs and block interferon signaling. Here we report the crystal structures of DDB1 alone and in complex with the simian virus 5 V protein. The DDB1 structure reveals an intertwined three-propeller cluster, which contains two tightly coupled β propellers with a large pocket in between and a third β propeller flexibly attached on the side. The rigid double-propeller fold of DDB1 is targeted by the viral V protein, which inserts an entire helix into the double-propeller pocket, whereas the third propeller domain docks DDB1 to the N terminus of the Cul4A scaffold. Together, these results not only provide structural insights into how the virus hijacks the DDB1-Cul4A ubiquitin ligase but also establish a structural framework for understanding the multiple functions of DDB1 in the uniquely assembled cullin-RING E3 machinery.**

## INTRODUCTION

Ubiquitin-dependent proteolysis is a widely used mechanism for eukaryotes to negatively modulate protein activities (Hershko and Ciechanover, 1998). Upon the attachment of a polyubiquitin chain, a protein substrate is targeted to the proteasome and can be effectively eliminated through proteasome-mediated degradation. Acting at the last step of a three-enzyme cascade (E1-E2-E3), ubiquitin-protein E3 ligases catalyze ubiquitin transfer from a ubiquitin-conjugating enzyme (E2) to the substrate and determine the specificity of the reaction (Pickart, 2001). The cullin-RING ubiquitin ligase complexes represent the largest superfamily of multisubunit E3s in eukaryotic cells (Petroski and Deshaies, 2005). In humans, six closely related cullin proteins (Cul1-3, 4A, 4B, and 5) have been identified, each capable of interacting with the RING finger protein Roc1 (also known as Rbx1 or Hrt1) and serving as the scaffold to assemble a distinct family of E3 complexes. The prototype of the cullin-RING E3s is the SCF (*S*kp1-*C*ul1-*F* box protein) complex, which is built upon Cul1-Roc1 and contains the Skp1 adaptor protein as well as a member of the F box protein family. Docked to the Cul1 scaffold by Skp1, the F box proteins can recruit diverse substrates to the SCF E3 machinery (Bai et al., 1996; Feldman et al., 1997; Skowyra et al., 1997). The modular architecture of SCF is apparently shared by several other cullin-RING E3 complexes. Cul2 and Cul5 are known to use elongin-C, a Skp1-homolog, as the adaptor for tethering the substrate binding VHL box and SOCS box proteins, whereas Cul3 has been demonstrated to directly interact with a family of substrate receptors through their common BTB domain, which has a Skp1-like structural fold (Petroski and Deshaies, 2005).

Unique among all cullins, Cul4A has recently been shown to form a stable complex with a 127 kDa cellular protein, DDB1, which shares no sequence homology with any cullin adaptor (Chen et al., 2001; Shiyanov et al., 1999). DDB1 is a multifunctional protein evolutionally conserved from fission yeast to humans (Tang and Chu, 2002). It was first isolated, together with DDB2, as a subunit of a heterodimeric protein complex that recognizes the UV-induced DNA lesions in the nucleotide excision repair pathway (Chu and Chang, 1988). Although DDB1 has subsequently been implicated in several other cellular functions, mounting evidence has now established a major role of DDB1 as a core subunit of the Cul4A-based ubiquitin ligase complex. This fundamental function of DDB1 in the E3 ligase is consistent with the strict coexistence of DDB1 and Cul4A in many eukaryotic species. To date, cellular proteins known as the substrates of the DDB1-Cul4A-Roc1 E3 include the yeast ribonucleotide reductase inhibitor Spd1, the metazoan DNA-replication licensing factor Cdt1, the mammalian transcription factor

c-Jun, and the human NER proteins DDB2 and XPC (Chen et al., 2001; Higa et al., 2003; Holmberg et al., 2005; Hu et al., 2004; Sugasawa et al., 2005; Wertz et al., 2004; Zhong et al., 2003). In complex with Cul4A, DDB1 has been proposed to either directly dock a substrate to the E3 machinery or indirectly recruit a substrate through an additional adaptor(s) (Sugasawa et al., 2005). Several cellular factors, including Det1, COP1, and the COP9 signalosome, have also been found in complex with DDB1-Cul4A-Roc1, regulating the ubiquitin ligase activities of the E3 (Groisman et al., 2003; Higa et al., 2003; Liu et al., 2003; Wertz et al., 2004).

Exploitation of the cullin-based ubiquitin ligases is a common strategy employed by various pathogenic viruses to ubiquitinate and degrade host factors crucial for combating or limiting viral infection (Banks et al., 2003; Petroski and Deshaies, 2005). Recent studies have shown that several paramyxoviruses, including simian virus 5 (SV5), mumps virus, and human parainfluenza virus type 2, are able to hijack the cellular DDB1-Cul4A-Roc1 E3 complex to promote the rapid degradation of the STAT proteins, which are the key signal transducers in the interferon pathway of antiviral response (Didcock et al., 1999; Parisien et al., 2001; Ulane and Horvath, 2002). A highly conserved V protein produced by these viruses directly binds to DDB1 and recruits STATs to the Cul4A-based E3 for ubiquitination (Andrejeva et al., 2002; Lin et al., 1998; Ulane and Horvath, 2002). In an effort to gain structural insights into the mechanisms underlying the ubiquitin ligase functions and the viral hijacking of the DDB1-Cul4A-Roc1 E3 machinery, we have determined the crystal structures of the full-length DDB1 in an isolated form and in complex with the full-length SV5 V protein (Table 1).

## RESULTS AND DISCUSSION

### Structure Determination

DDB1 was crystallized in space group $P2_12_12_1$, and its structure was solved at 3.0 Å resolution by mercury single-wavelength anomalous dispersion (SAD) (Table 1). Although the electron density map calculated from the SAD phases allowed unambiguous tracing of more than two-thirds of the polypeptide, confident building of a middle propeller domain (β propeller B) was limited to a backbone model due to its relatively poor densities. Crystals of this domain alone were subsequently obtained, and the structure was determined at 2.80 Å resolution by molecular replacement (MR). The DDB1-SV5-V complex was crystallized in space group $P2_1$ with two complexes in the asymmetric unit. The 2.85 Å resolution structure of the complex was determined by the MR method using the DDB1 middle propeller domain and the rest of the molecule as separate search models. Except for three presumably disordered loops (amino acids 1–15, 55–80, and 153–159), a structure model of the SV5 V protein bound to DDB1 was built with cycles of refinement and rebuilding.

### Structure Overview

The 127 kDa DDB1 protein forms a multidomain structure consisting of three seven-bladed β propellers (referred to as BPA to BPC for β propeller A to C) and a C-terminal helical domain (CTD) (Figure 1). The β propeller motif is a common protein fold characterized by multiple copies of a four-stranded antiparallel β sheet, which are twisted and radially packed around a central axis, analogous to the blades of a propeller (Jawad and Paoli, 2002; Pons et al., 2003). Apart from serving as catalytic enzymes for certain metabolic reactions, β propellers are frequently used as protein interaction modules by functionally diverse proteins (Smith et al., 1999). The three DDB1 β propeller domains are clustered together into a compact tristar structure, which is further supported by the CTD sitting next to the central joint region (Figure 1). BPA and BPC are closely coupled to each other face-to-face at an ~60° angle, resembling an open clam. A large empty pocket is formed between the two propellers. BPB, on the other hand, appears to be loosely tethered to BPC on its side through two pliable linker sequences. The flexibility of the connection between BPB and BPC is manifested by the drastically different orientations of BPB relative to the rest of the protein in the DDB1 and DDB1-SV5-V crystals (see below).

The SV5 V protein interacts with DDB1 through a bipartite structure, consisting of an N-terminal helical extension and a globular core domain stabilized by a novel zinc-finger motif (Figure 1). The SV5-V N-terminal helix is entirely engulfed by the large pocket formed between BPA and BPC, while the SV5-V core domain strengthens the interaction by packing against BPC on the opposite side where BPB is connected. Together, DDB1 and SV5-V form an elongated complex structure with a longest dimension of ~125 Å (Figure 1A).

### Propeller Cluster in DDB1

Based on the detection of 17 repeating sequence motifs, which are remotely related to the WD repeats, DDB1 has been previously predicted to have a multipropeller structure (Neuwald and Poleksic, 2000). The crystal structures show that the N-terminal 1045 residues of DDB1 indeed form three β propeller domains, all with the canonical seven-bladed fold (Figures 2A and 2B). Unexpectedly, the three propellers are not built in tandem in the polypeptide sequence. Instead, the sequence regions encoding BPA and BPB are separately inserted into the sequence of BPC, leading to a nonlinear domain arrangement. As a result, the polypeptide can be traced through the structure following the route of BPC→BPA→BPC→BPB→BPC→CTD (Figure 2B).

In the propeller cluster, BPA and BPB are connected to BPC via distinct mechanisms at the structural level. Conventionally, the blades of a propeller are numbered 1 to 7, and the four β strands of each blade are named a to d, from the inner to the outer ones (Lambright et al., 1996; Wall et al., 1995). With a conserved topology, the two opposite faces of the β propeller fold have been assigned as "top" and "bottom," each being lined with a specific set of loops connecting intra- and interblade strands (Figure 2B). In DDB1, BPA and BPC are joined through the "top" surface d-a loops of both propellers with two very short linkers. Through extensive interactions among the loops next to the linker regions, the two propellers are tightly packed to

**Table 1. Structure Determination and Refinement Statistics**

| Data Set | DDB1-Native | DDB1-EMP | DDB1-BPB | DDB1-SV5-V |
|---|---|---|---|---|
| Diffraction Data | | | | |
| Wavelength (Å) | 1.000 | 1.005 | 1.000 | 1.000 |
| Resolution (Å) | 50–3.0 | 50–3.1 | 50–2.80 | 50–2.85 |
| Observations | 122633 | 321250 | 174244 | 292780 |
| Unique reflections | 30258 | 29015 | 47189 | 78598 |
| Redundancy | 4.0 | 11.1 | 3.7 | 3.7 |
| Completeness (%) | 96.8 (95.9) | 99.6 (99.1) | 99.9 (100.0) | 99.4 (95.6) |
| Overall $I/\sigma$ | 18.9 (3.1) | 28.9 (3.6) | 32.4 (11.4) | 20.0 (2.4) |
| $R_{sym}$ (%) | 6.9 (38,3) | 11.1 (67.8) | 6.5 (15.5) | 5.9 (33.3) |
| Figure of merit | — | 0.42 | — | — |
| Refinement Statistics | | | | |
| Resolution limits (Å) | 50–3.00 | | 50–2.80 | 50–2.85 |
| Total Atoms | 8726 | | 9897 | 20407 |
| R-factor (%) | 24.4 | | 23.6 | 22.9 |
| R-free (%) | 30.7 | | 29.5 | 29.8 |
| RMSD bonds (Å) | 0.010 | | 0.007 | 0.009 |
| RMSD angles (°) | 1.87 | | 1.94 | 1.87 |
| Ramachandran Plot | | | | |
| Favored (%) | 95.9 | | 96.9 | 96.4 |
| Disallowed (%) | 0.0 | | 0.0 | 0.0 |

each other in a ''top'' to ''top'' fashion (Figures 2A and 2C). The relative positions of the two propellers are further secured by the CTD, which places a short helix right next to the propeller junction and inserts the side chain of Trp1073 between the two propeller domains (Figure 2C). Flanking this helix, two large loops in the CTD further hold the two propellers in place by interacting with their peripheral sides. Overall, these structural features of BPA, BPC, and the CTD present a clam-shaped double-propeller fold with a rigid appearance. Indeed, the overall structure of this double-propeller fold remains constant in both the free and viral protein bound forms of the DDB1 protein.

In contrast to BPA, BPB is only loosely attached to BPC on its side, making a limited number of contacts with the rest of the protein. The linkages between the two propellers are made through their c-d loops (1c and 1d of BPB to 2d and 2c of BPC, respectively), both located on the ''bottom'' faces, protruding away from the propeller cores (Figures 2B and 2D). The flexibility of the BPB-BPC connection was first suggested by the overall poor electron density of BPB in the DDB1 crystal, a crystallographic feature often associated with domains bearing considerable degrees of freedom within a protein. Subsequent superposition analysis of the DDB1 and the DDB1-SV5-V complex structures clearly revealed a hinge region in the BPB-BPC connection, as the BPB domain is differentially orientated relative to the rest of the protein in the two crystals (Figure 2E [compare with Figures 1A and 2A] and Figure S1). The two positions of BPB are corelated by a nearly 90° domain rotation around an axis along the longest dimension of the protein. Concurrent with this domain rearrangement, the BPB-BPC linker sequences undergo substantial conformational changes without disrupting the structures of the flanking β strands in the two propellers (Figure 2D). It is noteworthy that despite the substantial domain movement, a relatively constant BPB-BPC interdomain distance is maintained in the two structures. In fact, the amino acid sequences of the BPB-BPC linkers, especially between 2c of BPC and 1d of BPB, are highly conserved among DDB1 orthologs (Figure S2), suggesting that, even though the linkage between the two propeller domains is structurally flexible, the functions of DDB1 require a relatively close interpropeller connection, which has not been relaxed during evolution.

## Protein Interacting Sites of BPA-BPC

The clam-shaped structure formed by BPA and BPC presents a large pocket that can potentially bind DDB1-interacting partners. The space between the two domains is sandwiched by the ''top'' surface of each propeller, which is employed by most known β propellers for protein-protein interactions (Wilson et al., 2005). Distinct from BPA and BPB, whose ''top'' faces are fairly even, BPC sports three large

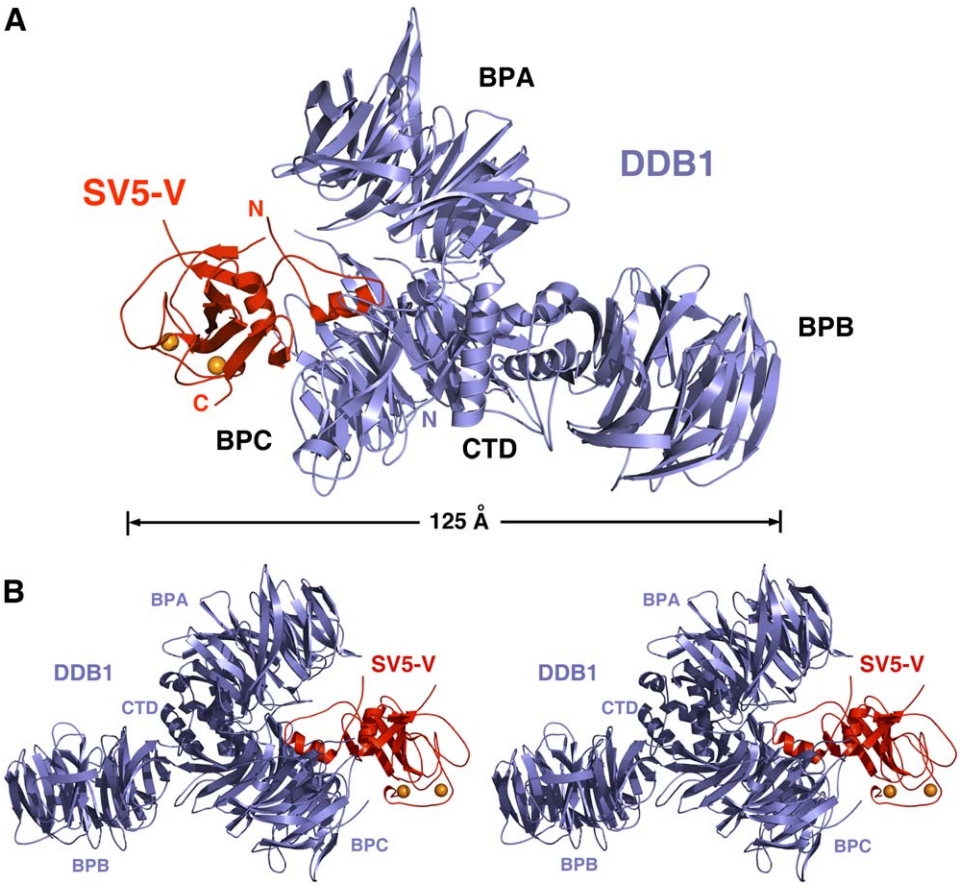


**Figure 1. The Simian Virus 5 V Protein Binds to DDB1, Which Adopts a Four-Domain Structure Consisting of a Three-Propeller Cluster and a Helical C-Terminal Domain**

(A) Overall view of the DDB1-SV5-V complex with DDB1 in blue and the SV5 V protein in red. The zinc ions in SV5-V are shown as orange spheres. The four DDB1 domains are labeled BPA, BPB, BPC, and CTD. The longest dimension of the complex is indicated.

(B) Stereo representation of the DDB1-SV5-V complex viewed from the opposite side as shown in (A).

consecutive b-c loops (2b-2c, 3b-3c, and 4b-4c loops), which protrude out on the top face of the propeller. In conjunction, these three BPC loops and the attached BPA and CTD domains create a ''wall'' surrounding three fourths of the top surface of the BPC domain and enclose an empty pocket of ~30 Å wide and ~30 Å deep among the three domains (Figure 3A). In contrast to the BPA side, the BPC side of the inside surface of the pocket is predominantly formed by aromatic and hydrophobic residues, which provide a hydrophobic environment suitable for protein-protein interactions (Figure 3B). Among these ''top'' surface residues of BPC, Trp953 and Met927, which are conserved in all DDB1 orthologs, are found near the opening of the pocket (Figure 3A). In the crystal of the DDB1-SV5-V complex, this DDB1 pocket accommodates the N-terminal helix of the viral protein, which mainly interacts with BPC.

Of the three large BPC b-c loops surrounding the pocket, loop 3b-3c is especially long and rich in Ser/Thr residues (Figures 2B and S2). In addition to extending the 3b and 3c strands on the top face of BPC, a major portion of this 45 amino acid loop folds back onto the domain and is tucked into the side of the propeller (Figure 3C). Intriguingly, a part of this loop sequence runs parallel with the entire 3d strand, creating a five-stranded β sheet in blade 3 (Figure 3C). The sequence encoding this structurally unique loop is found in the DDB1 orthologs of all animals (Figure S2), raising the possibility that this DDB1 loop might have functional roles remaining to be characterized.

In addition to using the top surface, the β propellers of several proteins with known structures also interact with their binding partners through the ''bottom'' and peripheral surfaces (Renault et al., 1998; Stamos et al., 2004). Structural analyses of BPA and BPC reveal several conserved surfaces on the bottom faces of both propellers as well as on one side of BPA (Figure S3), suggesting that additional protein-interacting sites are provided by the two domains. In particular, a number of solvent exposed residues, which are strictly conserved among metazoan DDB1 orthologs, are found clustered at the bottom surface of BPA, presenting a conserved surface groove leading to the other side of the propeller (Figure 3D). A functional role of this conserved surface is supported by the missense mutation of one of these

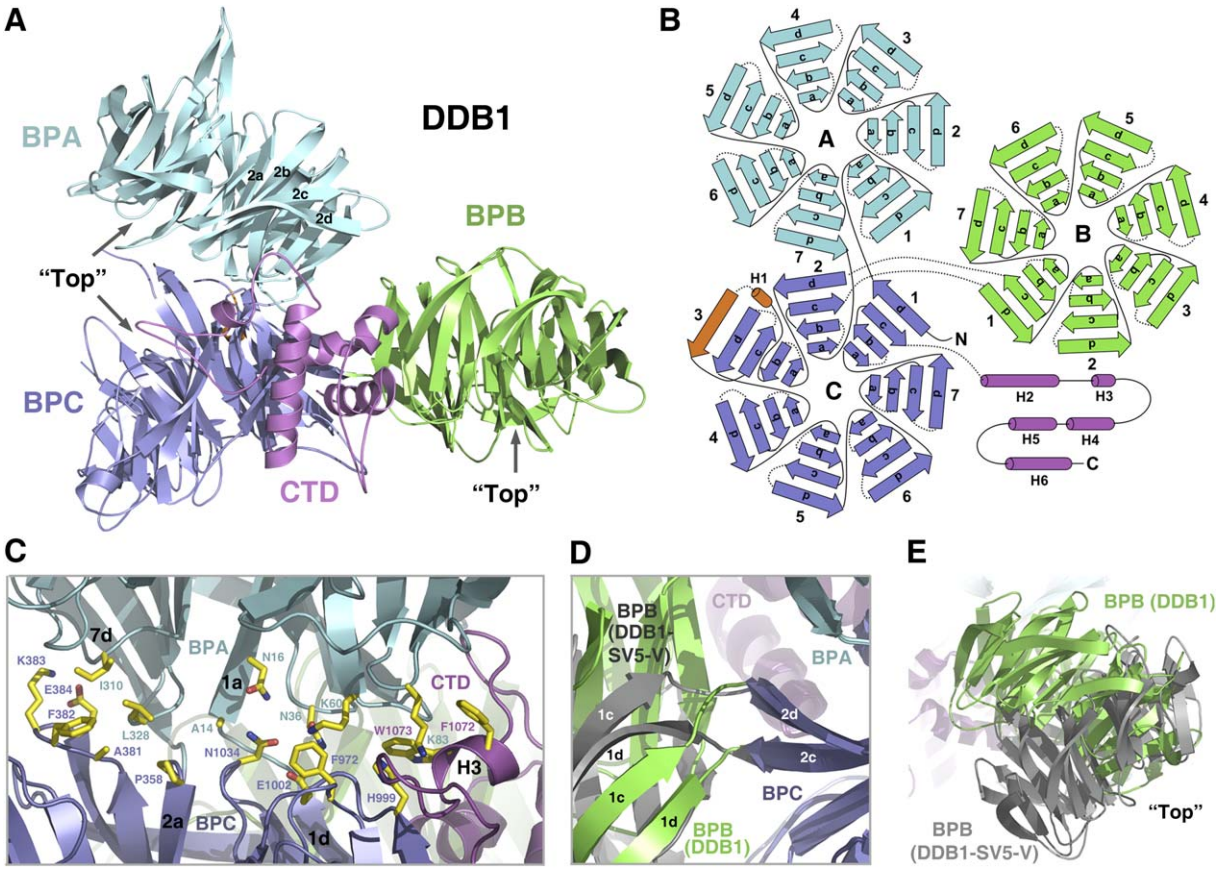


**Figure 2. The Propeller Cluster of DDB1 Contains Two Rigidly Coupled Seven-Bladed β Propeller Domains with a Third One Flexibly Attached**

(A) Structural domain arrangement of DDB1 as determined from the DDB1 crystal. The four domains of DDB1 are colored differently with the conventionally named top faces of each propeller indicated. The a-d strands of BPA's blade 2 are individually labeled.

(B) Schematic diagram of the secondary structure and domain arrangement of DDB1. The top surface loops of each propeller, which connect interblade d-a and b-c strands, are drawn in solid lines, whereas the bottom surface loops, which link intrablade a-b and c-d strands, are plotted in dash lines.

(C) The tight connection and the surrounding interface between BPA and BPC of DDB1. Only the domain-connecting strands are labeled. Side chains of the interacting residues from the two propeller domains are shown in sticks. The secondary structure elements and two key residues of the CTD, which interact with BPA and BPC, are shown at the lower right corner.

(D) The flexible connection between BPB and BPC revealed in the DDB1 and DDB1-SV5-V crystals. The BPB-BPC interpropeller connecting regions in the two crystal structures are shown, with the BPA, BPC, and CTD domains superimposed. The BPB domains in the two structures are colored differently.

(E) A side view of the BPB domains in the DDB1 and DDB1-SV5-V crystal structures with the rest of the proteins superimposed.

residues in the tomato DDB1 ortholog (Asn319 as the corresponding residue in human DDB1), which has recently been reported to be the cause of the *high pigment-1 (hp-1)* mutant phenotype of the plant (Lieberman et al., 2004; Liu et al., 2004). Intriguingly, another tomato mutant with a similar phenotype (*hp-1*$^{w}$) carries a missense mutation of a different DDB1 residue, which is mapped to the 4b-4c loop of BPC surrounding the double-propeller pocket (Glu842 as the corresponding residue in human DDB1, Figure S3A), implying that the functional role of the bottom surface of BPA might be in fact linked to that of the double-propeller pocket. Furthermore, mutations in the tomato homolog of Det1, which has been found interacting with DDB1, are to a large degree iso-phenotypic to *hp-1* (Levin et al., 2003; Mustilli et al., 1999), suggesting that the BPA-BPC double-propeller of DDB1 might play a role in Det1 binding. Indeed, when the DDB1 BPB domain alone and a DDB1 mutant lacking BPB were cotransfected with Det1 in 293T cells, Det1 specifically interacted with the latter, which contains the BPA-BPC double-propeller, but not with the BPB domain (Figure 3E). Precisely how DDB1 recruits Det1, however, remains to be revealed since equivalent plant *hp* mutations introduced in human DDB1 are not sufficient to disrupt the association between mammalian DDB1 and Det1 in cotransfected 293T cells (data not shown).

## BPB in DDB1-Cul4A Interaction

In addition to the BPA and BPC propellers, BPB provides yet another important protein interaction module in DDB1. A patch of seven residues, which are invariably conserved

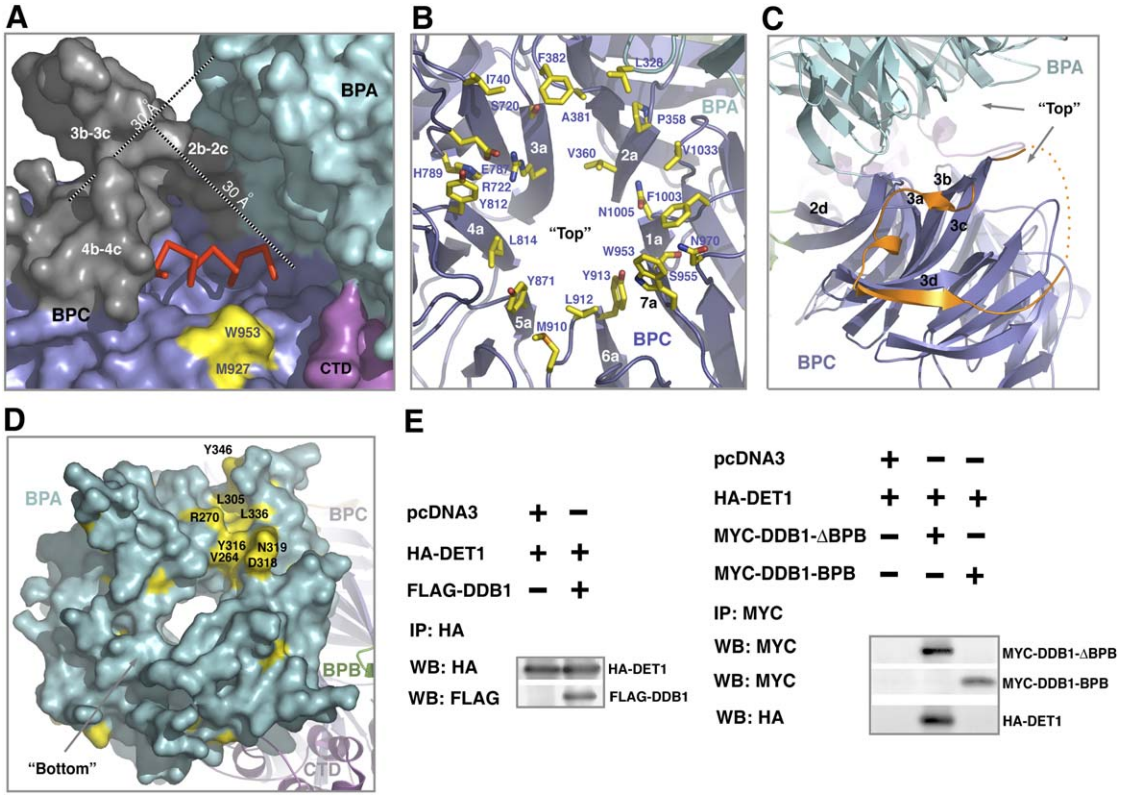


**Figure 3. Multiple Potential Protein Interaction Sites Are Found in the Double-Propeller Fold Formed by BPA and BPC of DDB1**

(A) Surface representation of DDB1's BPA-BPC double-propeller fold focusing on the large pocket enclosed between the top faces of the two propellers. The three long b-c loops of BPC forming a wall surrounding the pocket are colored in gray. Two surface residues strictly conserved in all DDB1 orthologs are colored in yellow. Approximate dimensions as well as a backbone representation of the interacting SV5-V helix are included to indicate the size of the pocket.

(B) The hydrophobic and aromatic residues on the "top" surface of BPC are shown in sticks.

(C) Ribbon representation of the unusual structure formed by the long 3b-3c loop of BPC (colored in orange) on one side of the propeller domain. The disordered region of the loop is shown in dash line.

(D) Surface representation of BPA showing the "bottom" surface of the domain with a patch of conserved residues exposed to the solvent. BPA residues that are strictly conserved among all metazoan DDB1 orthologs are colored in yellow. The rest of BPA domain is colored in cyan.

(E) Coimmunoprecipitation assays showing the association of Det1 with the BPA-BPC double-propeller fold of DDB1. The left panel shows the interaction between Det1 and the full-length DDB1 protein. The right panel shows the specific interaction between Det1 and the BPA-BPC double propeller fold. The indicated plasmids were transfected in 293T cells. One milligram of these lysates were immunoprecipitated with either the anti-HA antibody or the anti-MYC antibody and probed with the indicated antibodies for HA-DET1, FLAG-DDB1, MYC-DDB1-ΔBPB, and MYC-DDB1-BPB.

among all known DDB1 orthologs, is found on the top surface of BPB (Figure 4A). These residues define the largest continuous conserved surface area on the entire DDB1 protein (Figure S4), suggesting that they might participate in one of the most fundamental functions of DDB1 in the cell. Given that among all documented DDB1-interacting molecules Cul4A is the only protein strictly coexisting in parallel with DDB1 in the eukaryotic species, we speculated that the top surface of the BPB domain of DDB1 might be involved in Cul4A binding.

Our effort to map the binding domains between DDB1 and Cul4A in vivo by coimmunoprecipitation was complicated due to the presence of additional cellular factors that can interact with both proteins (e.g., the COP9 signalosome) (Liu et al., 2000, 2003). Therefore, we tested the direct binding between DDB1 and Cul4A in an in vitro GST pull-down assay with purified recombinant proteins. As expected, an isolated DDB1 BPB domain but not a DDB1 deletion mutant lacking BPB is able to form a stable complex with Cul4A (Figure S3C). Consistent with previously published results (Hu et al., 2004), the DDB1-BPB-interacting sites on Cul4A can be further mapped to the N-terminal domain of the cullin scaffold (Figure 4B). To confirm that the top surface of BPB represents the Cul4A binding site, we analyzed a number of BPB mutants with several conserved surface residues individually or simultaneously mutated to alanine. Strikingly, although mutations of two polar residues, Glu537 and Ser590, showed only limited effect on the complex formation, a single point mutation of Trp561, whose side chain is entirely exposed to the solvent, completely abolished the direct association between DDB1-BPB and Cul4-NTD (Figure 4C). These results strongly suggest that BPB anchors DDB1 to

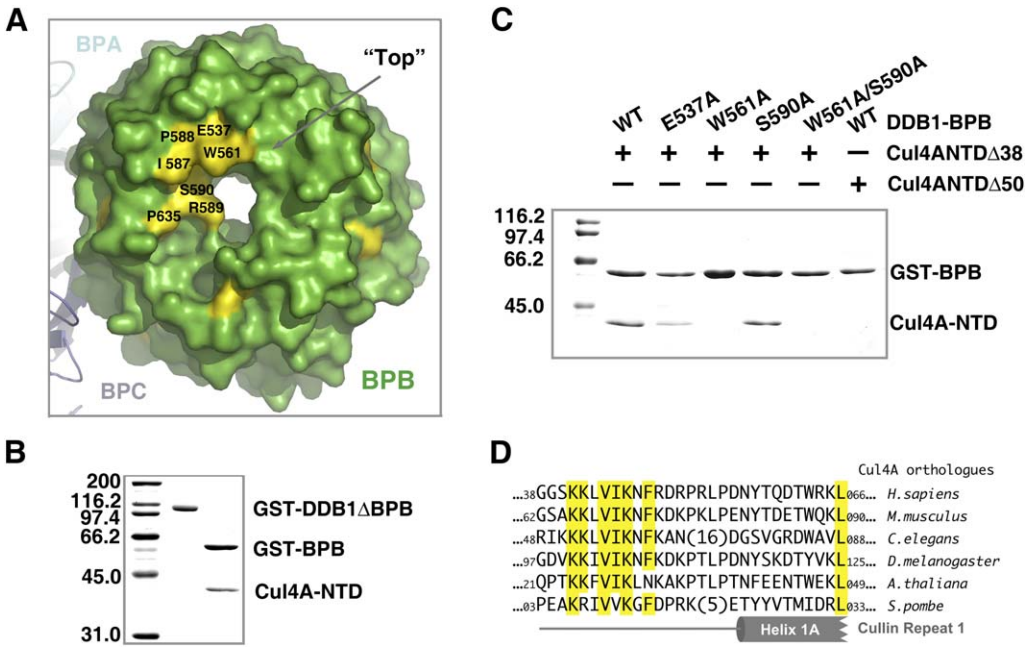


**Figure 4. Interactions between DDB1 and Cul4A Involve the Top Surface of the DDB1 BPB Domain and a Conserved Sequence Motif of Cul4A N-Terminal to the First Cullin Repeat**

(A) Surface representation of BPB showing the top surface of the domain with a patch of conserved residues exposed to the solvent. BPB residues that are strictly conserved among all DDB1 orthologs are colored in yellow, whereas the rest of the domain is colored in green.

(B) Mapping of the Cul4A-interacting structural unit of DDB1 by a GST pull-down assay.

(C) Mapping of the interacting residues in the DDB1 BPB domain and the NTD of Cul4A by mutagenesis and GST pull-down assays.

(D) A highly conserved sequence motif N-terminal to the predicted first cullin repeat of Cul4A. Strictly and predominantly conserved residues are highlighted in yellow. Sequences encoding the N-terminal half of the first helix in cullin repeat 1 of Cul4A are indicated by a cylinder underneath.

the NTD of the Cul4A scaffold through the top face of the propeller.

Based on the crystal structure of Cul1, the N-terminal domains of all cullins have been predicted to share a common elongated structure consisting of three consecutively packed five-helix cullin repeats (Zheng et al., 2002). Similar to Cul1, most cullins are known to use two specific helices in their first cullin repeat to bind a Skp1-like domain in their adaptors (Kamura et al., 2004; Pintard et al., 2003; Yu et al., 2004; Zheng et al., 2002). The absence of a Skp1/BTB/POZ fold in the DDB1 structure suggests that Cul4A-NTD interacts with DDB1 via a distinct structural mechanism. Previous studies have shown that deletion of the N-terminal 97 amino acids of Cul4A is sufficient to obliterate the DDB1-Cul4A complex formation (Hu et al., 2004). To further define the DDB1 binding sequence in the Cul4A NTD, we performed sequence alignment of the full-length Cul4A orthologs in conjunction with secondary structure prediction analysis. As shown in Figure 4D, a highly conserved K(K/R)(L/I/F)V(I/V)K motif can be found immediately N-terminal to the predicted first cullin repeat of all Cul4A orthologs. Deletion of this conserved sequence motif completely disrupted the direct interactions between Cul4A-NTD and DDB1-BPB (Figure 4C). In contrast, the removal of the very N-terminal nonconserved 38 amino acids of Cul4A showed no effect on DDB1 binding. The Cul4A-DDB1 interaction, therefore, is predominantly mediated by the short conserved sequence motif outside the cullin repeats of the cullin scaffold. We speculate that this Cul4A sequence motif directly binds to the conserved surface on the top face of the DDB1 BPB domain. Although the structural details of the DDB1-Cul4A interactions remain to be revealed, these lines of evidence demonstrate that the DDB1-Cul4A ubiquitin ligase complex is assembled via a novel mechanism distinct from that of other known cullin-based E3s. Cullin-RING ubiquitin ligase platforms, therefore, can be formed through a variety of mechanisms.

## Structure of the SV5 V Protein

As part of a bipartite structure, the SV5-V core domain is built around a central seven-stranded β sheet, which is sandwiched by one α helix and two long loops (Figure 5A). At one end of the β sheet, two large irregular loops coordinate two zinc ions via one histidine and seven cysteine residues, all of which are conserved among the V proteins of paramyxoviruses (Paterson et al., 1995). The resulting overall structure of SV5-V shares no significant structural homology with any known zinc binding proteins, representing a novel zinc-finger fold (Figures 5A and 5B and Figure S5). The V protein of SV5 is encoded by the viral P gene, which also produces the viral P protein upon RNA editing (Thomas et al., 1988). The SV5 V and P proteins share the same N-terminal

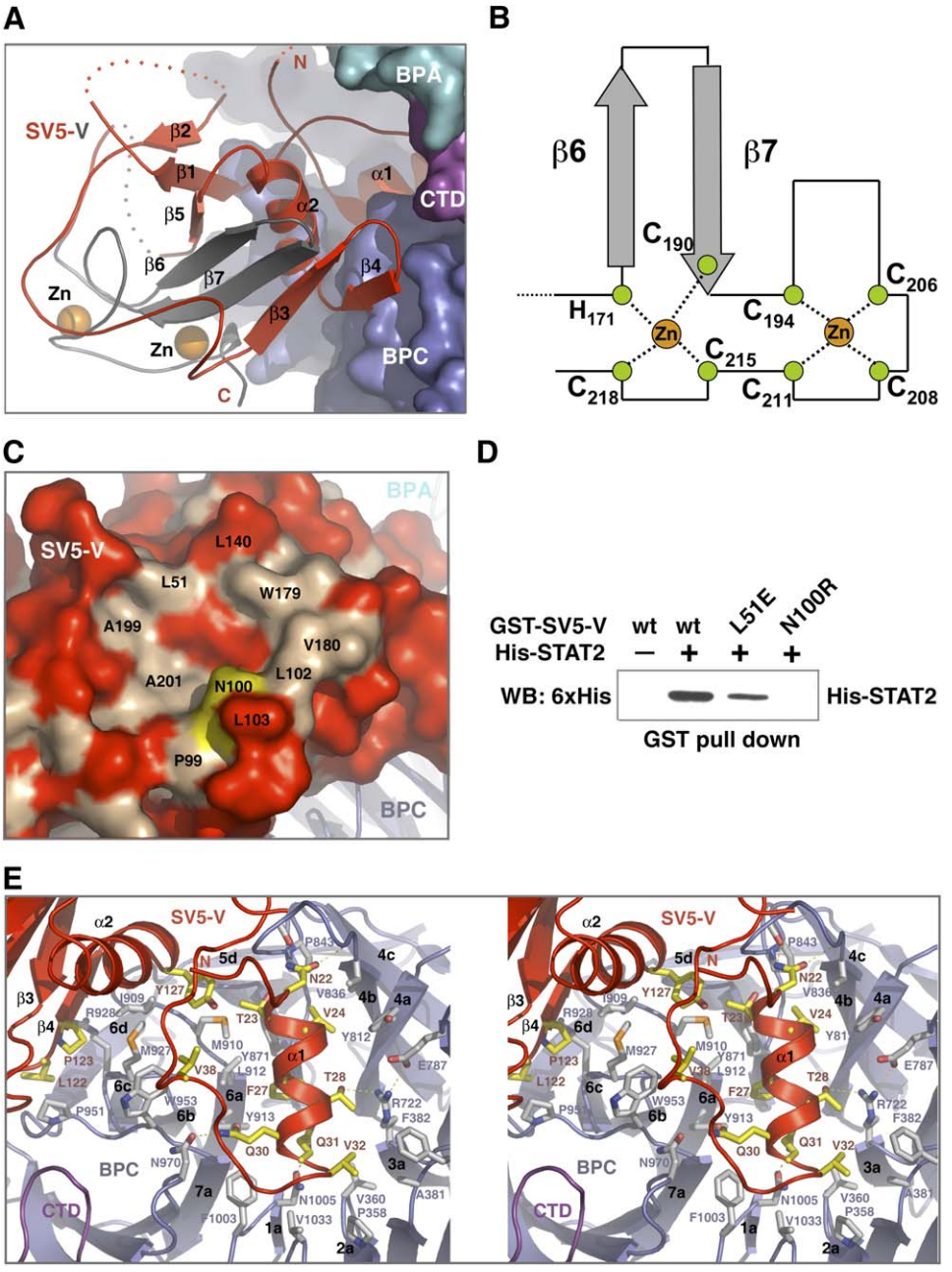


**Figure 5. The SV5 V Protein Adopts a Bipartite Structure upon Interacting with the DDB1 BPC Domain**

(A) Overall structure of the SV5 V protein in complex with DDB1. DDB1 and SV5-V are shown in surface and ribbon representation, respectively. The N-terminal part of the V protein, which is also found in the viral P protein, is colored in red. The rest of the V protein, including the zinc binding sequence, is colored in gray.

(B) A novel zinc-finger fold found in the SV5-V protein.

(C) Surface representation of SV5-V focusing on a bowl-shaped depression as a potential protein binding site. Residues conserved among the V proteins of SV5, human parainfluenza virus type 2, and mumps virus are colored in wheat. Two hydrophobic residues on the rim of the depression are also labeled. Asn100 is colored in yellow. The rest of the V protein is colored in red.

(D) GST pull-down assay showing that the potential protein binding site on the surface of the SV5 V protein is directly involved in STAT2 binding.

(E) Stereo view of the interface between SV5-V and the DDB1 BPC domain. Important DDB1-interacting residues in SV5-V are shown in yellow sticks, whereas the relevant SV5-V-interacting residues in DDB1 BPC are plotted in gray sticks.

164 amino acids sequence but are completely different in their C-terminal regions. The structure of SV5-V shows that its unique C-terminal sequence forms the middle two β strands as well as the zinc binding motif of the core domain (Figure 5A), all of which are crucial structural elements for the V protein to maintain its unique fold. Structurally independent of the core domain, the N-terminal 40 amino acids sequence of SV5-V adopts an α-helical structure with two flanking loops. This part of the V protein is almost entirely embedded in the pocket formed between the BPA and BPC domains of DDB1 (Figure 5A).

The solvent-exposed surface of the SV5-V core domain harbors a shallow bowl-shaped depression whose rim is almost exclusively formed by hydrophobic and nonpolar residues (Figure 5C). The hydrophobic features of most, if not all, of these residues are conserved among the paramyxovirus V proteins with demonstrated activities of ubiquitinating STATs. Although the polar Asn100 residue is exceptional in this group, its mutation to aspartic acid has been previously documented to confer on SV5 the ability to block interferon signaling in murine cells (Young et al., 2001), suggesting that it might directly participate in recruiting the STAT protein substrate. These lines of evidence, taken together, help reveal a potential protein binding site on SV5-V for tethering cellular substrates to DDB1. The SV5 V protein targets STAT1 for ubiquitination in a STAT2-dependent manner (Parisien et al., 2002b; Precious et al., 2005). Previous studies have shown that STAT2 not only forms a complex with SV5-V and STAT1 but also governs the host's range restriction of SV5 in human but not in mouse cells (Parisien et al., 2002a). The strict requirement of STAT2 for the function of the V protein suggests that SV5-V might bind STAT2 to recruit STAT1. In an in vitro GST pull-down assay, bacteria-produced recombinant STAT2 and SV5 can indeed directly interact with each other (Figure 5D). Importantly, mutation of Asn100 or a nearby conserved hydrophobic residue is able to essentially abolish or significantly weaken the STAT2-SV5-V interactions, confirming that the potential protein binding site of the viral V protein is involved in recruiting the STATs.

## SV5-DDB1 Interaction

The SV5 V protein binds to DDB1 using both its N-terminal extension and the core domain, burying a total of ~3730 Å$^2$ accessible protein surface area from the two proteins. Occupation of the BPA-BPC pocket of DDB1 by the N-terminal α1 helix of the V protein represents the hallmark of the viral-host protein interaction. SV5-V inserts its N-terminal helix into the DDB1 pocket with the C-terminal end of the helix pointing inward, barely reaching BPA (Figure 5E). Sitting in the middle of BPC's top surface, the SV5-V α1 helix packs its N-terminal end tightly against the long BPC 4b-4c loop, which appears to play an important role in sequestering the viral helix in the pocket (Figure 5E). The C-terminal end of the viral protein's α1 helix, meanwhile, interacts predominantly with the hydrophobic residues presented by BPC, making only limited van der Waal contacts with two amino acids in BPA. Overall, the entire viral protein helix forms extensive interfaces with the top surface of BPC throughout one side of the helical structure, as detailed in Figure 5E.

The formation of the DDB1-SV5-V complex is substantially reinforced by the core domain of the viral protein, which also interacts extensively with the DDB1 BPC domain. Binding to the opening of the DDB1 double-propeller pocket, the SV5-V core domain is in contact with the BPC 4b-4c loop on one side and the CTD on the other, thereby completing the formation of a 360° wall surrounding the center of BPC's top face (Figure 5A). The major interactions between the SV5-V core domain and BPC are mediated by the viral protein's β4 strand, which runs along the edge of the BPC top face (Figure 5E). Next to the β4 strand, a conserved tyrosine residue in the SV5-V's α2 helix makes multiple van der Waals contacts with the BPC loops as well as the viral N-terminal α1 helix (Figure 5E). Upon interacting with DDB1, SV5-V induces slight conformational changes in the BPC blades that are in close contact with the viral protein core domain, yet the majority of the DDB1 BPA-BPC double-propeller fold remains essentially unchanged (with a 1.04 Å rmsd for 789 residues in the free and viral bound forms). The critical roles played by both the N-terminal extension and the core domain of the viral protein in DDB1 binding are underscored by the undetectable interactions of DDB1 with SV5-V mutants lacking either end of the polypeptide (Andrejeva et al., 2002). The requirement of both the N-terminal helix and the integrity of the core domain for the complex formation between the viral protein and DDB1 provides a structural explanation for the specific capability of the viral V but not P protein to hijack the cellular DDB1-Cul4A-Roc1 E3 machinery (Didcock et al., 1999).

The N-terminal sequence shared between the paramyxovirus V and P proteins has been previously reported to be natively disordered in an isolated form (Karlin et al., 2002). Recognition of the V protein's N-terminal extension by DDB1, therefore, most likely involves an induced fit mechanism. Besides hijacking DDB1, SV5-V has been implicated to have several other functions (Andrejeva et al., 2004; Lin et al., 1997; Randall and Bermingham, 1996). It is possible that upon binding to other cellular factors, the N-terminal extension of SV5-V might adopt a different structure(s). Such structural plasticity is expected to be essential for the versatility of many viral proteins.

## Implications for the Multiple Functions of DDB1 in the E3

Distinct from all other known cullin adaptors and substrate receptors, DDB1 has a triple-propeller cluster structure, which presents and spatially organizes multiple protein-protein interaction sites with the longest dimension reaching ~100 Å. These structural features of DDB1 conceivably underlie its many functions in the Cul4A-based E3 machinery. Using the BPB domain, DDB1 directly interacts with Cul4A to assemble the E3 platform. Through several other protein-interacting sites, including the double-propeller pocket, DDB1 can recruit diverse cellular substrates to the ubiquitin ligase complex. With its longest dimension matching that of the cullin scaffold, DDB is presumably capable of presenting

and positioning the substrates to the Roc1 bound E2 for ubiquitination. Moreover, equipped with multiple ligand binding sites, DDB1 is able to dock additional regulators to the E3 machinery besides substrates. Recent studies have reported that an E2 variant protein COP10, which can modulate the activities of the canonical E2 enzymes, was found in the same complex with *Arabidopsis* DDB1 and Det1 (Yanagawa et al., 2004), suggesting that the cognate E2 of the DDB1-Cul4A-Roc1 E3 ligase can be regulated for differential ubiquitin chain assembly, at least in plants. Finally, the unusual ligand binding capacity of DDB1 might allow it to target the ubiquitin ligase complex to special subcellular locations such as the damaged-DNA site and the centromere (Groisman et al., 2003; Obuse et al., 2004). Despite the detailed DDB1 structures obtained in the current studies, how DDB1 forms a complex with DDB2 and participates in the recognition of the UV DNA lesions remains to be revealed. How the ubiquitin ligase activities of the DDB1-Cul4A-Roc1 E3 might be coupled to its localization to UV-damaged DNA also waits to be answered. The current structures of DDB1 provide a structural framework for addressing these questions and unravelling the structural basis of the multiple functional roles of the protein in the E3 complex.

### Flexibility within a Cullin-Based E3 Complex

The DDB1 structure represents the first case where an obvious hinge region is revealed in a subunit of a cullin-based E3 complex. Previous structural studies have shown that several subcomplexes of the SCF and SCF-like E3s are characterized by apparently rigid architectures. It has been proposed that the cullin-based E3 machinery might partially mediate the ubiquitination reaction by optimally positioning the substrates relative to the E2 (Schulman et al., 2000; Zheng et al., 2002). Distinct from these complexes, DDB1 displays a flexible linkage between the major protein binding module (BPA-BPC) and the cullin binding domain (BPB). Minor contacts between Cul4A and DDB1 beyond the DDB1 BPB domain might exist and be able to lock the domain configuration of DDB1. Alternatively, the BPA-BPC double propeller might be indirectly anchored on Cul4A by additional binding proteins, which can limit the flexibility of DDB1. Nevertheless, we speculate that the flexible domain connection in DDB1 can be functionally favored in the DDB1-Cul4A E3. For instance, the flexibility of DDB1 might be important for it to present substrates bound at different sites to the E2. The hinge movement of the DDB1 domains might also play a role in the assembly of a specific ubiquitin chain when a cofactor such as COP10 is present. With the domain architecture of DDB1 revealed, the importance of the hinge region in the E3 and the functional significance of limited flexibility in the cullin E3s in general can now be formally tested.

### Implications for Other Multipropeller Proteins

The multipropeller fold has been recognized in numerous functionally diverse proteins (He et al., 2004; Komuro et al., 2004; Zou et al., 1997). The DDB1 structures reported here present both opportunities and challenges for elucidating the structural basis of their functions. On the one hand, the DDB1 structure can be directly used to model the spliceosome-associated protein 130 (SAP130) in the U2 snRNP particle and the largest subunit of the cleavage and polyadenylation specificity factor (CPSF160), both of which are essential components of eukaryotic messenger RNA-processing machines and share significant sequence homology with DDB1 throughout their entire polypeptides (Figure S6) (Neuwald and Poleksic, 2000). A homology model of SAP130 will likely help locate the protein in the structure of the SF3b subcomplex of U2 snRNP determined by cryoelectron microscopy (Golas et al., 2003). On the other hand, the intertwined propeller domain arrangement and the differential interpropeller structural coupling as revealed in the DDB1 structure show unexpected complexities involved in the folding and structural organization of multiple propeller domains. Such complexities add a new level of challenges to the structural prediction and modeling of multipropeller proteins.

## Conclusions

Our studies show that the evolutionally conserved DDB1 protein adopts a striking intertwined three-propeller fold, featuring multiple protein binding sites exquisitely organized in space. Distinct from all known cullin adaptors, DDB1 assembles with Cul4A-Roc1 through a novel mechanism, forming a unique cullin-RING ubiquitin ligase platform. In order to divert the E3 function of the DDB1-Cul4A-Roc1 complex for its own use, the paramyxovirus V protein binds to a prominent double-propeller pocket on DDB1, altering its substrate recognition properties by presenting a STAT-interacting site. Together with biochemical evidence, these results have established the structural framework essential for obtaining mechanistic understanding of the functions of DDB1-Cul4A E3 in various cellular pathways.

## EXPERIMENTAL PROCEDURES

### Protein Overexpression and Purification

Full-length human DDB1 was overexpressed as a glutathione S-transferase (GST)-fusion protein in insect cells. Full-length SV5-V and the DDB1 BPB domain (amino acids 391–709) were overexpressed as GST-fusion proteins in *E. coli*. All proteins were isolated from the soluble cell lysate by glutathione affinity chromatography. After cleavage by TEV, all proteins were further purified by anion exchange and gel filtration chromatography and concentrated by ultrafiltration. The DDB1-SV5-V complex was isolated on a Superdex 200 gel filtration column with a mixture of the two proteins at a 1:1.5 molar ratio. All protein samples were in a final solution of 20 mM Tris-HCl (pH = 8.0), 200 mM NaCl, and 5 mM dithiothreitol (DTT).

### Crystallization and Data Collection

All crystals were grown at 4°C by the hanging drop vapor diffusion method with 1.5 μl protein samples mixed with an equal volume of reservoir solutions. The purified DDB1 protein (5.6 mg/ml) was crystallized with a reservoir solution containing 100 mM MES (pH = 6.5), 15%–17% PEG 4000, 50 mM NaCl, and 5 mM DTT. The DDB1 crystals form in space group $P2_12_12_1$ (a = 63.4 Å, b = 133.8 Å, c = 184.7 Å) and contain one molecule in the asymmetric unit. The purified DDB1-BPB domain (8 mg/ml) was crystallized with a reservoir solution containing 100 mM HEPES (pH = 7.5), 19%–21% PEG 4000, 10% isopropanol, and 5 mM DTT. The DDB1-BPB crystals form in space group $P2_1$ (a = 101.7 Å, b = 73.9 Å, c = 137.1 Å, and β = 111.7°) and contain four molecules in the asymmetric unit. The purified DDB1-SV5-V protein complex (6 mg/ml) was crystallized

with a reservoir solution containing 100 mM BTP (pH = 7.5), 19%–21% PEG 20000, 50 mM NaCl, and 5 mM DTT. The DDB1-SV5-V crystals form in space group $P2_1$ (a = 62.7 Å, b = 240.8 Å, c = 117.2 Å, and β = 101.8º) and contain two complexes in the asymmetric unit. A DDB1 mercury derivative crystal was prepared by soaking the crystal in the reservoir solution supplemented with 1 mM ethyl mercuric phosphate (EMP) for 12 hr. All the data sets were collected at the BL5.0.2 beamline at the Advanced Light Source in Berkeley using crystals flash-frozen in the crystallization buffers supplemented with 15%–20% glycerol at −170ºC. Reflection data were indexed, integrated, and scaled (Table 1) using the HKL2000 package (Otwinowski and Minor, 1997).

### Structure Determination and Refinement

The native crystal structure of DDB1 was determined by mercury SAD using the EMP-derivatized crystal. Fifteen mercury sites were located using SOLVE (Terwilliger and Berendzen, 1999). After improving the phases by solvent-flattening using RESOLVE (Terwilliger, 2000) on the basis of a solvent content of 50%, interpretable electron density maps were obtained. A native date set of the DDB1 crystal was collected to 3.0 Å resolution and used for model building and refinement with O and CNS (Brunger et al., 1998; Jones et al., 1991). Due to the poor electron densities of the BPB domain, only a polyalanine model was initially built for this part of DDB1. With the crystals of isolated DDB1 BPB domain and the available polyalanine model, the structure of DDB1-BPB was determined by molecular replacement (MR) in conjunction with molecular averaging. Iterative cycles of model building, averaging, density modification, and restrained refinement were performed using O, CNS, and the CCP4 programs (CCP4, 1994). The final BPB model was refined to 2.80 Å. The crystal structure of the DDB1-SV5-V complex was also determined by MR, using the DDB1-BPB domain structure and the model of the rest of the protein as separate search models in AmoRe (CCP4, 1994). 3.0 Å electron density maps calculated with phases derived from the rigid-body-refined DDB1 model had clearly interpretable density for the most part of SV5-V. SV5-V was built into the difference density upon numerous cycles of manual-building/rebuilding and refinement (simulated annealing, positional, and grouped B factor) with CNS. The entire complex structure was refined to 2.85 Å and has been checked using simulated annealing composite omit maps. The final refined model of the DDB1-SV5-V protein does not contain one DDB1 loop (amino acids 774–779) and three SV5-V loops (amino acids 1–15, 55–80, and 153–159) due to the absence of their electron densities. It is assumed that these loops are disordered in the crystal. All figures were prepared with PyMol (DeLano, 2002) and rendered either internally or by PovRay.

### Site-Directed Mutagenesis and GST Pull-Down Assays

The GST-Cul4A-Roc1 complex was overexpressed and purified from insect cells following the same procedures previously reported for preparing recombinant Cul1-Roc1 (Zheng et al., 2002). GST-DDB1-BPB, GST-DDB1-ΔBPB, and 6xHis-STAT2 fusion proteins were overproduced and purified from *E. coli*. Cul4A-NTD, Cul4A-NTDΔ38, and Cul4A-NTD-Δ50 (amino acid 401 as the common C-terminal boundary) were prepared following the same method for preparing DDB1-BPB. Site-directed mutagenesis of DDB1-BPB and SV5-V was carried out using the Quickchange kit (Stratagene). Previously reported procedures were followed for the GST pull-down experiments (Zheng et al., 2002).

### Supplemental Data

Supplemental Data include six figures and can be found with this article online at http://www.cell.com/cgi/content/full/124/1/105/DC1/.

## ACKNOWLEDGMENTS

We thank ALS synchrotron beamline staff for assistance with data collection; Raymond J. Deshaies and all members of the Zheng lab for invaluable discussions; R.E. Randall at the University of St. Andrews for SV5-V plasmid; and Wenqing Xu, William A. Catterall, and Joseph A. Beavo for help and support in our research. N.Z. is a Pew scholar. This study is supported by NIH grant CA107134 to N.Z. and CA098210 to P.Z.

Received: June 6, 2005
Revised: August 16, 2005
Accepted: October 11, 2005
Published: January 12, 2006

## REFERENCES

Andrejeva, J., Poole, E., Young, D.F., Goodbourn, S., and Randall, R.E. (2002). The p127 subunit (DDB1) of the UV-DNA damage repair binding protein is essential for the targeted degradation of STAT1 by the V protein of the paramyxovirus simian virus 5. J. Virol. *76*, 11379–11386.

Andrejeva, J., Childs, K.S., Young, D.F., Carlos, T.S., Stock, N., Goodbourn, S., and Randall, R.E. (2004). The V proteins of paramyxoviruses bind the IFN-inducible RNA helicase, mda-5, and inhibit its activation of the IFN-beta promoter. Proc. Natl. Acad. Sci. USA *101*, 17264–17269.

Bai, C., Sen, P., Hofmann, K., Ma, L., Goebl, M., Harper, J.W., and Elledge, S.J. (1996). SKP1 connects cell cycle regulators to the ubiquitin proteolysis machinery through a novel motif, the F-box. Cell *86*, 263–274.

Banks, L., Pim, D., and Thomas, M. (2003). Viruses and the 26S proteasome: hacking into destruction. Trends Biochem. Sci. *28*, 452–459.

Brunger, A.T., Adams, P.D., Clore, G.M., DeLano, W.L., Gros, P., Grosse-Kunstleve, R.W., Jiang, J.S., Kuszewski, J., Nilges, M., Pannu, N.S., et al. (1998). Crystallography & NMR system: A new software suite for macromolecular structure determination. Acta Crystallogr. D Biol. Crystallogr. *54*, 905–921.

CCP4. (1994). The CCP4 Suite: programs for protein crystallography. Acta Crystallogr. D Biol. Crystallogr. *D50*, 760–763.

Chen, X., Zhang, Y., Douglas, L., and Zhou, P. (2001). UV-damaged DNA-binding proteins are targets of CUL-4A-mediated ubiquitination and degradation. J. Biol. Chem. *276*, 48175–48182.

Chu, G., and Chang, E. (1988). Xeroderma pigmentosum group E cells lack a nuclear factor that binds to damaged DNA. Science *242*, 564–567.

DeLano, W.L. (2002). The PyMOL User's Manual (San Carlos: DeLano Scientific).

Didcock, L., Young, D.F., Goodbourn, S., and Randall, R.E. (1999). The V protein of simian virus 5 inhibits interferon signalling by targeting STAT1 for proteasome-mediated degradation. J. Virol. *73*, 9928–9933.

Feldman, R.M., Correll, C.C., Kaplan, K.B., and Deshaies, R.J. (1997). A complex of Cdc4p, Skp1p, and Cdc53p/cullin catalyzes ubiquitination of the phosphorylated CDK inhibitor Sic1p. Cell *91*, 221–230.

Golas, M.M., Sander, B., Will, C.L., Luhrmann, R., and Stark, H. (2003). Molecular architecture of the multiprotein splicing factor SF3b. Science *300*, 980–984.

Groisman, R., Polanowska, J., Kuraoka, I., Sawada, J., Saijo, M., Drapkin, R., Kisselev, A.F., Tanaka, K., and Nakatani, Y. (2003). The ubiquitin ligase activity in the DDB2 and CSA complexes is differentially regulated by the COP9 signalosome in response to DNA damage. Cell *113*, 357–367.

He, X., Semenov, M., Tamai, K., and Zeng, X. (2004). LDL receptor-related proteins 5 and 6 in Wnt/beta-catenin signaling: arrows point the way. Development *131*, 1663–1677.

Hershko, A., and Ciechanover, A. (1998). The ubiquitin system. Annu. Rev. Biochem. *67*, 425–479.

Higa, L.A., Mihaylov, I.S., Banks, D.P., Zheng, J., and Zhang, H. (2003). Radiation-mediated proteolysis of CDT1 by CUL4–ROC1 and CSN complexes constitutes a new checkpoint. Nat. Cell Biol. *5*, 1008–1015.

Holmberg, C., Fleck, O., Hansen, H.A., Liu, C., Slaaby, R., Carr, A.M., and Nielsen, O. (2005). Ddb1 controls genome stability and meiosis in fission yeast. Genes Dev. *19*, 853–862.

Hu, J., McCall, C.M., Ohta, T., and Xiong, Y. (2004). Targeted ubiquitination of CDT1 by the DDB1–CUL4A-ROC1 ligase in response to DNA damage. Nat. Cell Biol. *6*, 1003–1009.

Jawad, Z., and Paoli, M. (2002). Novel sequences propel familiar folds. Structure (Camb) *10*, 447–454.

Jones, T.A., Zou, J.Y., Cowan, S.W., and Kjeldgaard (1991). Improved methods for building protein models in electron density maps and the location of errors in these models. Acta Crystallogr A *47 (Pt 2)*, 110–119.

Kamura, T., Maenaka, K., Kotoshiba, S., Matsumoto, M., Kohda, D., Conaway, R.C., Conaway, J.W., and Nakayama, K.I. (2004). VHL-box and SOCS-box domains determine binding specificity for Cul2-Rbx1 and Cul5-Rbx2 modules of ubiquitin ligases. Genes Dev. *18*, 3055–3065.

Karlin, D., Longhi, S., Receveur, V., and Canard, B. (2002). The N-terminal domain of the phosphoprotein of Morbilliviruses belongs to the natively unfolded class of proteins. Virology *296*, 251–262.

Komuro, A., Masuda, Y., Kobayashi, K., Babbitt, R., Gunel, M., Flavell, R.A., and Marchesi, V.T. (2004). The AHNAKs are a class of giant propeller-like proteins that associate with calcium channel proteins of cardiomyocytes and other cells. Proc. Natl. Acad. Sci. USA *101*, 4053–4058.

Lambright, D.G., Sondek, J., Bohm, A., Skiba, N.P., Hamm, H.E., and Sigler, P.B. (1996). The 2.0 A crystal structure of a heterotrimeric G protein. Nature *379*, 311–319.

Levin, I., Frankel, P., Gilboa, N., Tanny, S., and Lalazar, A. (2003). The tomato dark green mutation is a novel allele of the tomato homolog of the DEETIOLATED1 gene. Theor. Appl. Genet. *106*, 454–460.

Lieberman, M., Segev, O., Gilboa, N., Lalazar, A., and Levin, I. (2004). The tomato homolog of the gene encoding UV-damaged DNA binding protein 1 (DDB1) underlined as the gene that causes the high pigment-1 mutant phenotype. Theor. Appl. Genet. *108*, 1574–1581.

Lin, G.Y., Paterson, R.G., and Lamb, R.A. (1997). The RNA binding region of the paramyxovirus SV5 V and P proteins. Virology *238*, 460–469.

Lin, G.Y., Paterson, R.G., Richardson, C.D., and Lamb, R.A. (1998). The V protein of the paramyxovirus SV5 interacts with damage-specific DNA binding protein. Virology *249*, 189–200.

Liu, C., Powell, K.A., Mundt, K., Wu, L., Carr, A.M., and Caspari, T. (2003). Cop9/signalosome subunits and Pcu4 regulate ribonucleotide reductase by both checkpoint-dependent and -independent mechanisms. Genes Dev. *17*, 1130–1140.

Liu, W., Nichols, A.F., Graham, J.A., Dualan, R., Abbas, A., and Linn, S. (2000). Nuclear transport of human DDB protein induced by ultraviolet light. J. Biol. Chem. *275*, 21429–21434.

Liu, Y., Roof, S., Ye, Z., Barry, C., van Tuinen, A., Vrebalov, J., Bowler, C., and Giovannoni, J. (2004). Manipulation of light signal transduction as a means of modifying fruit nutritional quality in tomato. Proc. Natl. Acad. Sci. USA *101*, 9897–9902.

Mustilli, A.C., Fenzi, F., Ciliento, R., Alfano, F., and Bowler, C. (1999). Phenotype of the tomato high pigment-2 mutant is caused by a mutation in the tomato homolog of DEETIOLATED1. Plant Cell *11*, 145–157.

Neuwald, A.F., and Poleksic, A. (2000). PSI-BLAST searches using hidden markov models of structural repeats: prediction of an unusual sliding DNA clamp and of beta-propellers in UV-damaged DNA-binding protein. Nucleic Acids Res. *28*, 3570–3580.

Obuse, C., Yang, H., Nozaki, N., Goto, S., Okazaki, T., and Yoda, K. (2004). Proteomics analysis of the centromere complex from HeLa interphase cells: UV-damaged DNA binding protein 1 (DDB-1) is a component of the CEN-complex, while BMI-1 is transiently co-localized with the centromeric region in interphase. Genes Cells *9*, 105–120.

Otwinowski, Z., and Minor, W., eds. (1997). Processing of X-ray Diffraction Data Collected in Oscillation Mode (New York: Academic Press).

Parisien, J.P., Lau, J.F., Rodriguez, J.J., Sullivan, B.M., Moscona, A., Parks, G.D., Lamb, R.A., and Horvath, C.M. (2001). The V protein of human parainfluenza virus 2 antagonizes type I interferon responses by destabilizing signal transducer and activator of transcription 2. Virology *283*, 230–239.

Parisien, J.P., Lau, J.F., and Horvath, C.M. (2002a). STAT2 acts as a host range determinant for species-specific paramyxovirus interferon antagonism and simian virus 5 replication. J. Virol. *76*, 6435–6441.

Parisien, J.P., Lau, J.F., Rodriguez, J.J., Ulane, C.M., and Horvath, C.M. (2002b). Selective STAT protein degradation induced by paramyxoviruses requires both STAT1 and STAT2 but is independent of alpha/beta interferon signal transduction. J. Virol. *76*, 4190–4198.

Paterson, R.G., Leser, G.P., Shaughnessy, M.A., and Lamb, R.A. (1995). The paramyxovirus SV5 V protein binds two atoms of zinc and is a structural component of virions. Virology *208*, 121–131.

Petroski, M.D., and Deshaies, R.J. (2005). Function and regulation of cullin-RING ubiquitin ligases. Nat. Rev. Mol. Cell Biol. *6*, 9–20.

Pickart, C.M. (2001). Mechanisms underlying ubiquitination. Annu. Rev. Biochem. *70*, 503–533.

Pintard, L., Willis, J.H., Willems, A., Johnson, J.L., Srayko, M., Kurz, T., Glaser, S., Mains, P.E., Tyers, M., Bowerman, B., and Peter, M. (2003). The BTB protein MEL-26 is a substrate-specific adaptor of the CUL-3 ubiquitin-ligase. Nature *425*, 311–316.

Pons, T., Gomez, R., Chinea, G., and Valencia, A. (2003). Beta-propellers: associated functions and their role in human diseases. Curr. Med. Chem. *10*, 505–524.

Precious, B., Young, D.F., Andrejeva, L., Goodbourn, S., and Randall, R.E. (2005). In vitro and in vivo specificity of ubiquitination and degradation of STAT1 and STAT2 by the V proteins of the paramyxoviruses simian virus 5 and human parainfluenza virus type 2. J. Gen. Virol. *86*, 151–158.

Randall, R.E., and Bermingham, A. (1996). NP:P and NP:V interactions of the paramyxovirus simian virus 5 examined using a novel protein:protein capture assay. Virology *224*, 121–129.

Renault, L., Nassar, N., Vetter, I., Becker, J., Klebe, C., Roth, M., and Wittinghofer, A. (1998). The 1.7 A crystal structure of the regulator of chromosome condensation (RCC1) reveals a seven-bladed propeller. Nature *392*, 97–101.

Schulman, B.A., Carrano, A.C., Jeffrey, P.D., Bowen, Z., Kinnucan, E.R., Finnin, M.S., Elledge, S.J., Harper, J.W., Pagano, M., and Pavletich, N.P. (2000). Insights into SCF ubiquitin ligases from the structure of the Skp1-Skp2 complex. Nature *408*, 381–386.

Shiyanov, P., Nag, A., and Raychaudhuri, P. (1999). Cullin 4A associates with the UV-damaged DNA-binding protein DDB. J. Biol. Chem. *274*, 35309–35312.

Skowyra, D., Craig, K.L., Tyers, M., Elledge, S.J., and Harper, J.W. (1997). F-box proteins are receptors that recruit phosphorylated substrates to the SCF ubiquitin-ligase complex. Cell *91*, 209–219.

Smith, T.F., Gaitatzes, C., Saxena, K., and Neer, E.J. (1999). The WD repeat: a common architecture for diverse functions. Trends Biochem. Sci. *24*, 181–185.

Stamos, J., Lazarus, R.A., Yao, X., Kirchhofer, D., and Wiesmann, C. (2004). Crystal structure of the HGF beta-chain in complex with the Sema domain of the Met receptor. EMBO J. *23*, 2325–2335.

Sugasawa, K., Okuda, Y., Saijo, M., Nishi, R., Matsuda, N., Chu, G., Mori, T., Iwai, S., Tanaka, K., and Hanaoka, F. (2005). UV-induced ubiquitylation of XPC protein mediated by UV-DDB-ubiquitin ligase complex. Cell *121*, 387–400.

Tang, J., and Chu, G. (2002). Xeroderma pigmentosum complementation group E and UV-damaged DNA-binding protein. DNA Repair (Amst.) *1*, 601–616.

Terwilliger, T.C. (2000). Maximum-likelihood density modification. Acta Crystallogr. D Biol. Crystallogr. *56*, 965–972.

Terwilliger, T.C., and Berendzen, J. (1999). Automated MAD and MIR structure solution. Acta Crystallogr. D Biol. Crystallogr. *55*, 849–861.

Thomas, S.M., Lamb, R.A., and Paterson, R.G. (1988). Two mRNAs that differ by two nontemplated nucleotides encode the amino coterminal proteins P and V of the paramyxovirus SV5. Cell *54*, 891–902.

Ulane, C.M., and Horvath, C.M. (2002). Paramyxoviruses SV5 and HPIV2 assemble STAT protein ubiquitin ligase complexes from cellular components. Virology *304*, 160–166.

Wall, M.A., Coleman, D.E., Lee, E., Iniguez-Lluhi, J.A., Posner, B.A., Gilman, A.G., and Sprang, S.R. (1995). The structure of the G protein heterotrimer Gi alpha 1 beta 1 gamma 2. Cell *83*, 1047–1058.

Wertz, I.E., O'Rourke, K.M., Zhang, Z., Dornan, D., Arnott, D., Deshaies, R.J., and Dixit, V.M. (2004). Human De-etiolated-1 regulates c-Jun by assembling a CUL4A ubiquitin ligase. Science *303*, 1371–1374.

Wilson, D.K., Cerna, D., and Chew, E. (2005). The 1.1-angstrom structure of the spindle checkpoint protein Bub3p reveals functional regions. J. Biol. Chem. *280*, 13944–13951.

Yanagawa, Y., Sullivan, J.A., Komatsu, S., Gusmaroli, G., Suzuki, G., Yin, J., Ishibashi, T., Saijo, Y., Rubio, V., Kimura, S., et al. (2004). Arabidopsis COP10 forms a complex with DDB1 and DET1 in vivo and enhances the activity of ubiquitin conjugating enzymes. Genes Dev. *18*, 2172–2181.

Young, D.F., Chatziandreou, N., He, B., Goodbourn, S., Lamb, R.A., and Randall, R.E. (2001). Single amino acid substitution in the V protein of simian virus 5 differentiates its ability to block interferon signaling in human and murine cells. J. Virol. *75*, 3363–3370.

Yu, Y., Xiao, Z., Ehrlich, E.S., Yu, X., and Yu, X.F. (2004). Selective assembly of HIV-1 Vif-Cul5-ElonginB-ElonginC E3 ubiquitin ligase complex through a novel SOCS box and upstream cysteines. Genes Dev. *18*, 2867–2872.

Zheng, N., Schulman, B.A., Song, L., Miller, J.J., Jeffrey, P.D., Wang, P., Chu, C., Koepp, D.M., Elledge, S.J., Pagano, M., et al. (2002). Structure of the Cul1-Rbx1-Skp1-F boxSkp2 SCF ubiquitin ligase complex. Nature *416*, 703–709.

Zhong, W., Feng, H., Santiago, F.E., and Kipreos, E.T. (2003). CUL-4 ubiquitin ligase maintains genome stability by restraining DNA-replication licensing. Nature *423*, 885–889.

Zou, H., Henzel, W.J., Liu, X., Lutschg, A., and Wang, X. (1997). Apaf-1, a human protein homologous to C. elegans CED-4, participates in cytochrome c-dependent activation of caspase-3. Cell *90*, 405–413.

## Accession Numbers

The Protein Data Bank accession numbers for the DDB1-SV5-V, DDB1, and DDB1 BPB domain structures are 2B5L, 2B5M, and 2B5N.